Coene et al., http://www.jcb.org/cgi/content/full/jcb.201004136/DC1

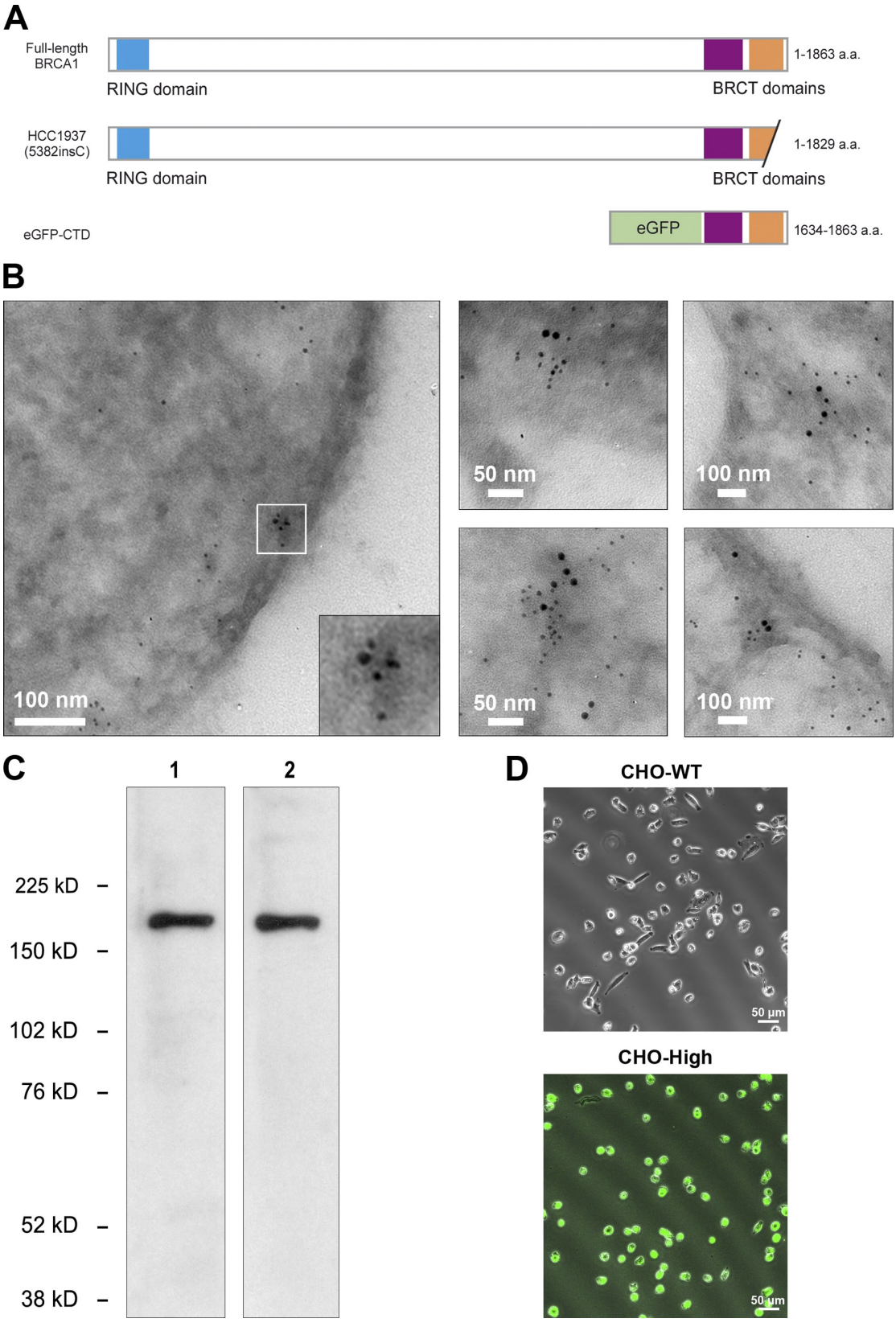

Figure S1. **Schematic presentation of the BRCA1 BRCT domains, cryoimmuno-EM of PMA-stimulated HeLa cells, Western blot of CHO cells, and spreading of CHO-WT versus CHO-High cells.** (A) Schematic presentation of the BRCA1 BRCT domains. Full-length BRCA1 contains two conserved C-terminal BRCT domains. The HCC1937 cell line harbors a 5382insC mutation that leads to a premature stop codon at 1,829. This results in a truncated BRCA1 protein, which is missing part of the second BRCT domain. EGFP-CTD represents the construct that was used as a dominant-negative fusion protein. It contains EGFP in frame with both intact BRCA1 BRCT domains. (B) Cryoimmuno-EM of PMA-stimulated HeLa cells. Thawed ultrathin cryosections were labeled for detection of ERM proteins and BRCA1 using anti-ERM and anti-BRCA1 Ab4 primary antibodies and 10-nm and 5-nm gold-conjugated secondary antibodies, respectively. Colocalization of both labels was observed at the PM (left, inset). Additional smaller snapshots showing this colocalization are included (right). (C) Western blot of CHO cells. Western blot analysis of CHO lysate using anti-Ser988 (1) and anti-Ser1497 (2) BRCA1 antibodies. A single protein band of the correct size was detected. (D) Spreading of CHO-WT versus CHO-High cells. CHO-WT and CHO-High cells were seeded and fixed after a 3-h incubation time. We observed more spread out cells for the CHO-WT than for the CHO-High cell population.

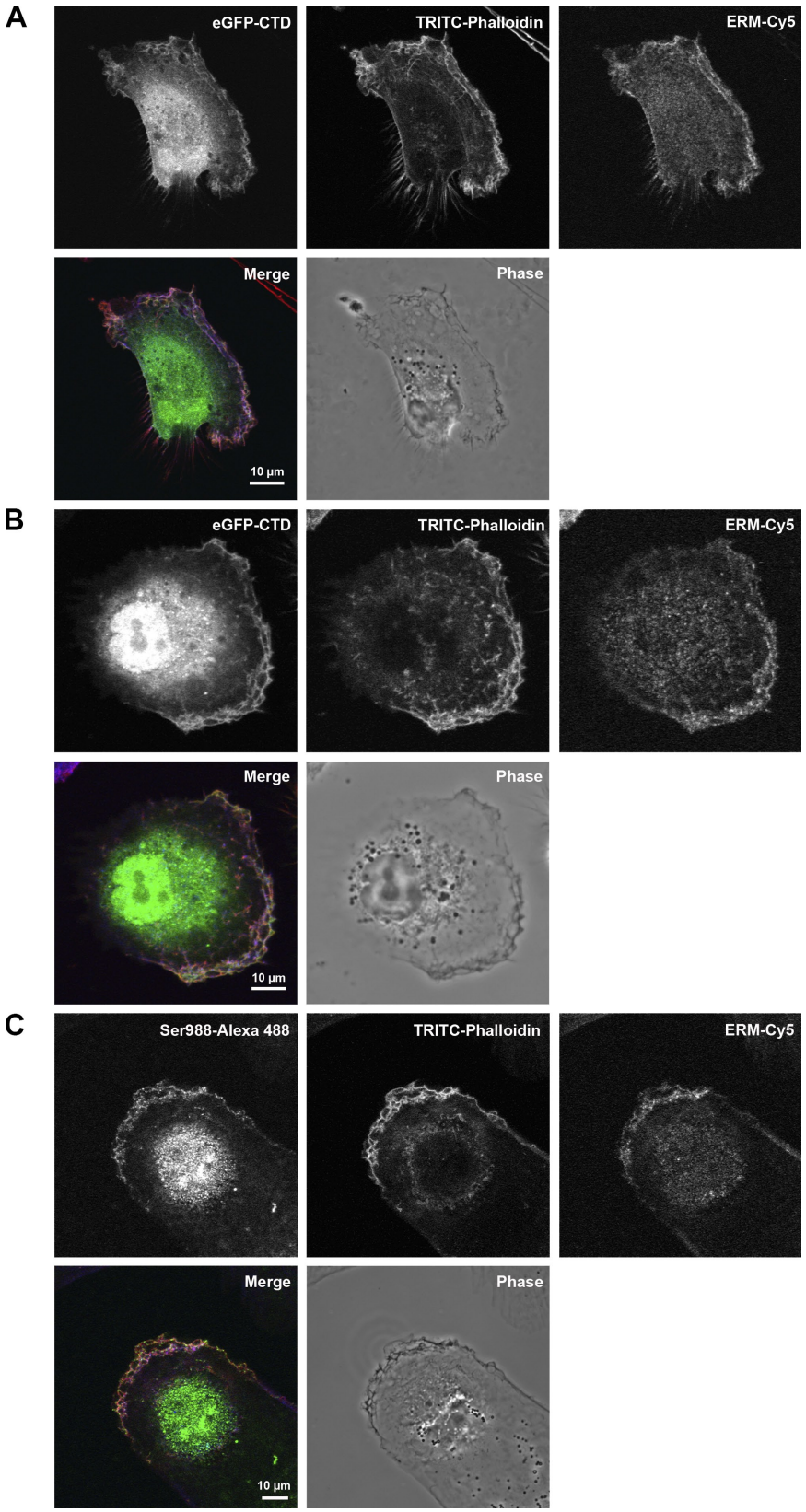

Figure S2. **EGFP-CTD and endogenous BRCA1 colocalization with F-actin and ERM.** (A and B) CLSM of double immunofluorescence labeling of transiently EGFP-BRCA1$^{1634–1863}$ (EGFP-CTD)–expressing HCC1937 (A) and PMA-stimulated HeLa (B) cells with TRITC-phalloidin (F-actin) and anti-ezrin–radixin–moesin (ERM) antibody (Cy5). Colocalization was observed at the membrane ruffles. (C) Triple immunofluorescence labeling of HCC1937 cells with anti-Ser988 BRCA1 antibody (Alexa Fluor 488), anti-ERM antibody (Cy5), and TRITC-phalloidin (F-actin) also showed colocalization of all three proteins at the membrane ruffles. Phase images are also shown.

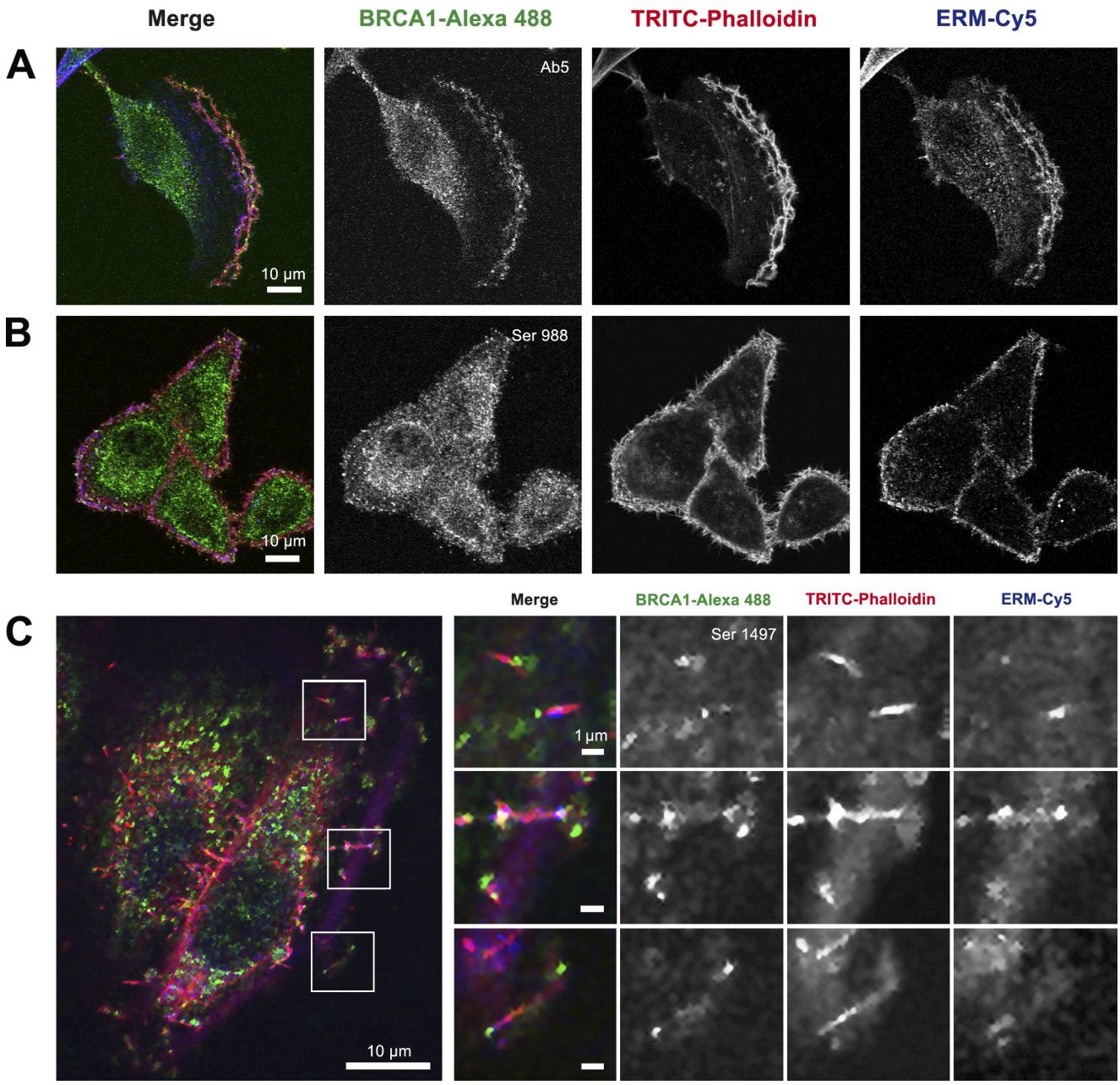

Figure S3. **Endogenous BRCA1 colocalization with F-actin and ERM.** (A–C) CLSM of triple immunofluorescence labeling of HCC1937 (A), HeLa (B), and ECV304 (C) cells with anti-BRCA1 antibodies (Alexa Fluor 488) Ab5 (A), Ser988 (B), and Ser1497 (C), TRITC-phalloidin (F-actin), and anti-ezrin–radixin–moesin (ERM) antibody (Cy5). Colocalization of BRCA1, F-actin, and ERM was observed at membrane ruffles in the leading edge (A), PM (B), and PM extensions (C). (C, right) Higher magnifications of three ROIs (left, insets) are presented showing the specific BRCA1–ERM–F-actin spatial organization.

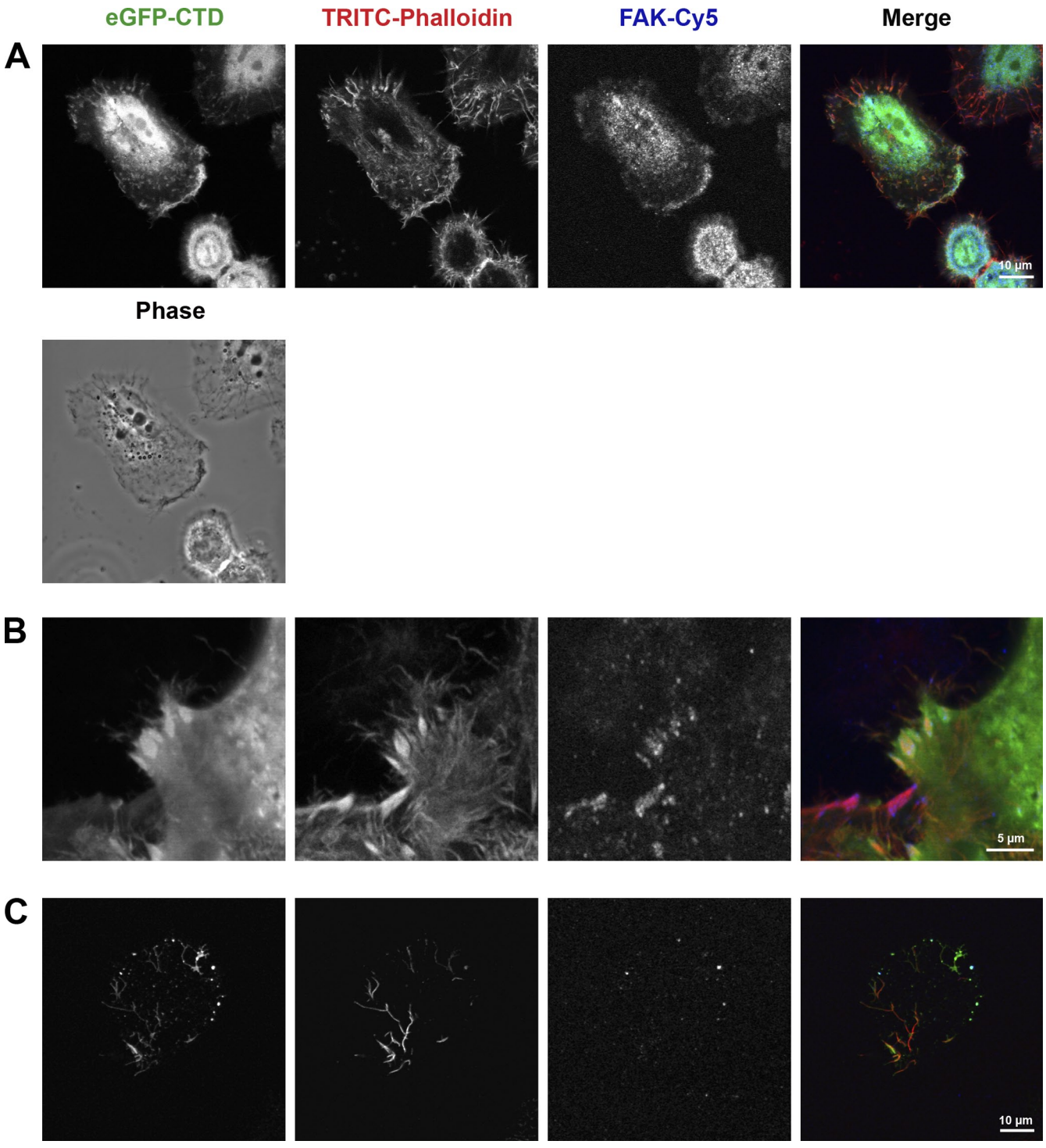

Figure S4. **EGFP-CTD is present in focal adhesion plaques.** CLSM of double immunofluorescence labeling of transiently EGFP-BRCA1$^{1634–1863}$ (EGFP-CTD)–expressing HeLa cells with TRITC-phalloidin (F-actin) and anti-FAK antibody (Cy5). (A–C) Colocalization was observed at the membrane ruffles (A), in focal adhesion plaques (B), and in cellular footprints after mechanical removal of the cells (C). The phase image is shown for A.

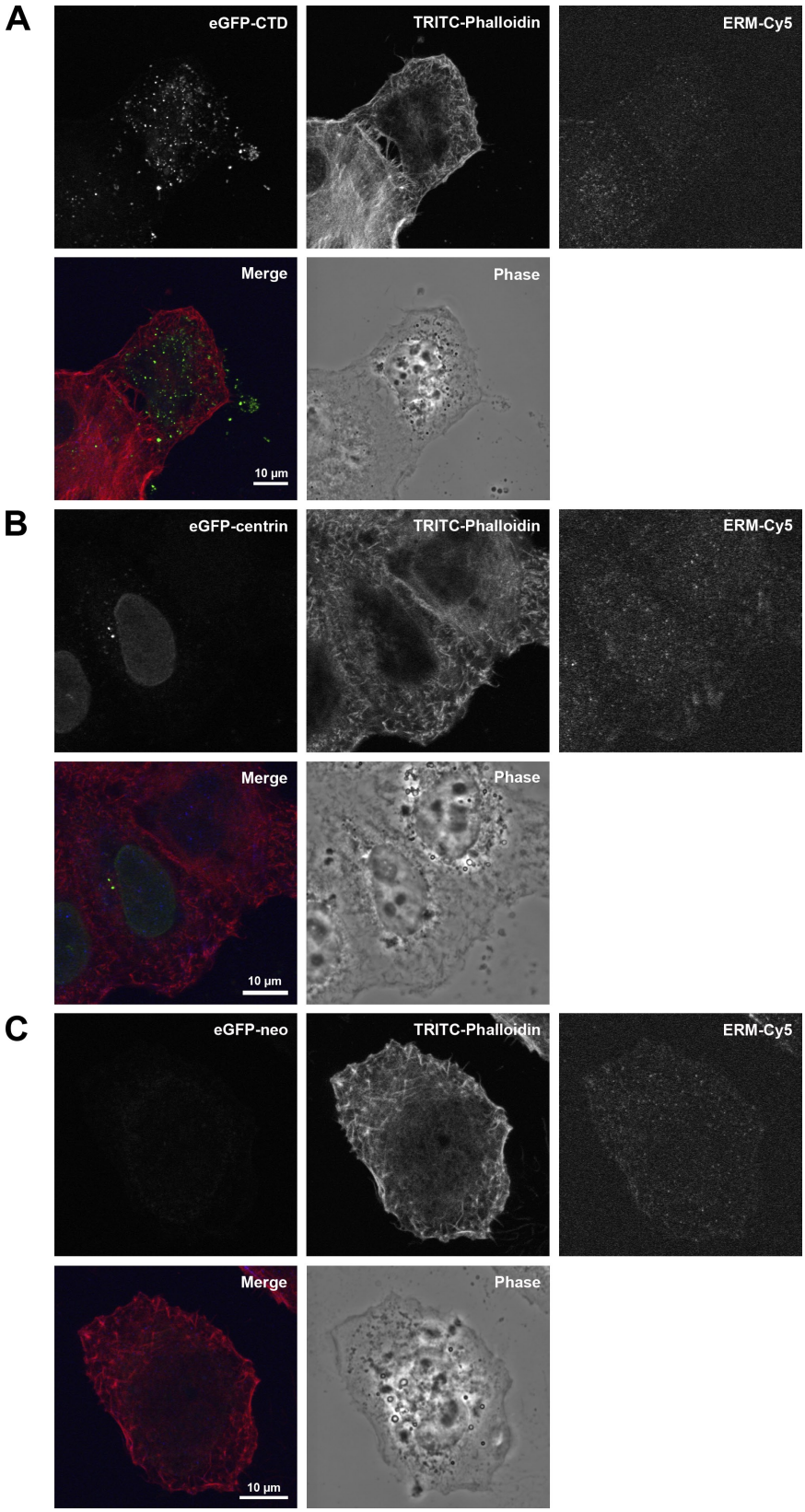

Figure S5. **EGFP-protein distribution after saponin treatment.** (A–C) CLSM of double immunofluorescence labeling of PMA-stimulated HeLa cells transiently expressing EGFP-BRCA1$^{1634–1863}$ (EGFP-CTD; A), EGFP-centrin (B), and EGFP-neo (C) with TRITC-phalloidin (F-actin) and anti-ezrin–radixin–moesin (ERM) antibody (Cy5) after saponin treatment. (A) Specific focal labeling with EGFP-CTD persisted, often in association with F-actin, whereas saponin damage to membrane ruffles appeared to remove both the EGFP-CTD and anti-ERM labels from these structures. (B) No peripheral focal label was seen in EGFP-centrin–expressing cells after saponin treatment, whereas targeted protein expression was confirmed by the presence of duplicated perinuclear centrioles. (C) In cells expressing soluble EGFP, no signal persisted after saponin treatment. Phase images are also shown.

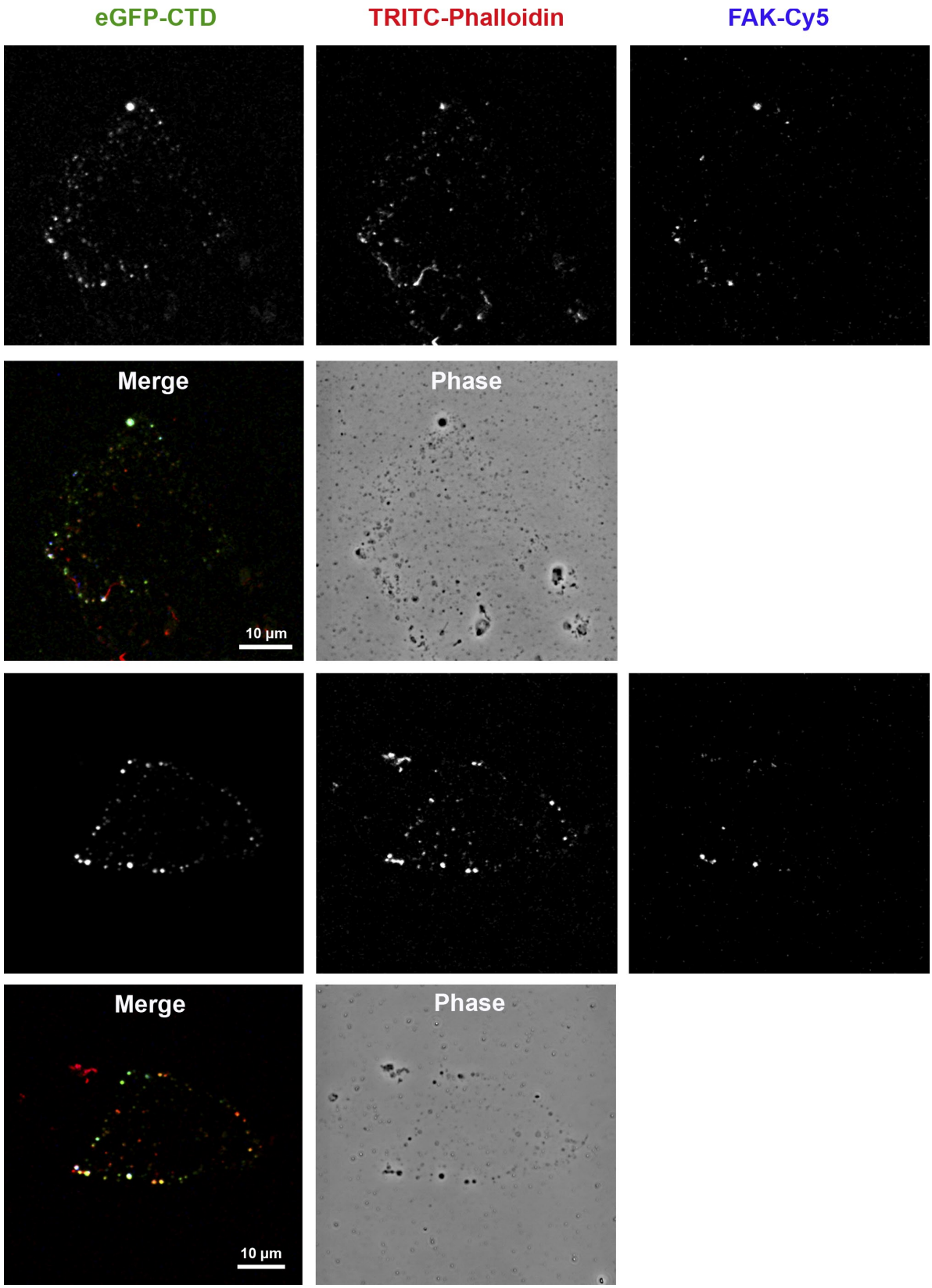

Figure S6. **Colocalization of EGFP-CTD, F-actin, and FAK after saponin treatment.** CLSM of double immunofluorescence labeling of transiently EGFP-BRCA1$^{1634–1863}$ (EGFP-CTD)–expressing, PMA-stimulated HeLa cells with TRITC-phalloidin and anti-FAK antibody (Cy5) after saponin treatment. No PM labeling for EGFP-CTD was detected because of saponin-damaged membrane ruffles, but colocalization of all three proteins was observed in the remaining saponin-resistant focal adhesion plaques, resulting in a white color. Phase images are shown.

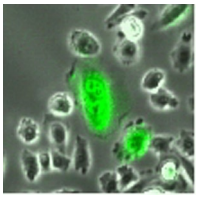

Video 1. **PM dynamics.** 4-h time course of a CHO–EGFP-BRCA1$^{1634–1863}$ high expressing cell, imaged at 2-min intervals, showed the dynamic behavior of moving membrane ruffles, which were strongly positive for the fusion protein. Playback speed, seven frames per second. Nonconfocal phase contrast, EGFP fluorescence, and merged images are shown.

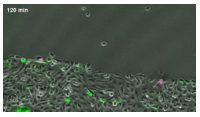

Video 2. **Wound healing: loss of cell–cell contacts and enhanced invasion capacity.** 11-h time course of unsorted CHO–EGFP-BRCA1$^{1634–1863}$ (CHO-EGFP) cells, imaged at 2-min intervals and sampled every two frames, showed the enhanced invasion capacity of single cells (orange track). The pink tracks point at loss of cell–cell contact and detachment of cells that are migrating away from the front line into the wound. Tracks were obtained using ImageJ and MTrackJ (National Institutes of Health). Playback speed, 12 frames per second. Nonconfocal phase contrast and EGFP fluorescence merged images are shown.

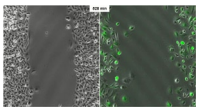

Video 3. **Wound healing.** 12-h time course of a wound-healing assay, which was imaged at 2-min intervals: CHO–wild type (CHO-WT) versus CHO cells stably expressing high levels of EGFP-BRCA1$^{1634–1863}$ (CHO-High). Stacks were sampled every two frames and reduced 95% in x and y. The front lines of the CHO-WT wound moved forward as one and showed a more regular behavior than CHO-High. CHO-High showed more irregular wound healing, with more cells loosing cell–cell contact and moving individually into the wound. Playback speed, 12 frames per second. Nonconfocal phase contrast and EGFP fluorescence merged images are shown.

Table S1. **1D SDS-PAGE ligand overlay blotting of HeLa P2 fractions: LC-MS/MS results**

Gel band and protein ID	Swiss-Prot number	Mass	Mascot score
		kD	
1			
4F2	P08195	57,909	603
Ezrin	P15311	69,239	242
Radixin	P35241	68,521	149
HS90B	P08238	83,081	136
GLU2B	P14314	59,259	98
HS90A	P07900	84,490	87
AAAT	Q15758	56,562	78
2			
GRP78	P11021	72,288	1,293
4F2	P08195	57,909	477
Radixin	P35241	68,521	178
Moesin	P26038	67,647	166
Ezrin	P15311	69,225	118
PDIA4	P13667	72,887	114
GRP75	P38646	73,635	93
FKB10	Q96AY3	64,204	90
SCRB1	Q8WTV0	60,838	88

Per gel band, the corresponding protein IDs, Swiss-Prot numbers, mass, and Mascot scores are presented. Only proteins above Mascot score 70 were shown. The first protein per gel band represents the highest Mascot score in the analyzed sample. The background score is 35.

Table S2. **2D electrophoresis ligand overlay blotting of HeLa P2 fractions: LC-MS/MS results**

Gel spot and protein ID	Swiss-Prot number	Mass	Mascot score
		kD	
1			
Moesin	P26038	67,761	202
2			
Moesin	P26038	67,761	409
3			
Moesin	P26038	67,892	724
Ezrin	P15311	69,470	221
4			
Radixin	P35241	68,635	227
Moesin	P26038	67,761	130
5			
Radixin	P35241	68,635	211
Moesin	P26038	67,761	176
T-complex protein 1 γ subunit	P49368	61,066	111
6			
Ezrin	P15311	69,353	278
Radixin	P35241	68,635	110
7			
LEG7	P47929	14,992	93
H4	P62805	11,229	80
S10A9	P06702	13,291	70
S10A8	P05109	10,885	69
Ezrin	P15311	69,339	57
8			
Ezrin	P15311	69,353	189

Per gel spot, the corresponding protein IDs, Swiss-Prot numbers, mass, and Mascot scores are displayed. Only proteins above Mascot score 55 were shown. The first protein per gel spot represents the highest Mascot score in the analyzed sample. The background score is 35.